Soft Matter

PAPER

View Article Online
View Journal | View Issue

Cite this: *Soft Matter*, 2023, **19**, 3946

Nonlinear chemical reaction induced abnormal pattern formation of chemotactic particles†

Xianyun Jiang, Huijun Jiang* and Zhonghuai Hou *

Received 1st November 2022,
Accepted 15th May 2023

DOI: 10.1039/d2sm01433e

rsc.li/soft-matter-journal

The chemotactic behavior of particles is a widespread and important phenomenon that enables them to interact with the chemical species present in the environment. These chemical species can undergo chemical reactions and even form some non-equilibrium chemical structures. In addition to chemotaxis, particles can also produce or consume chemicals, which allows them to further couple with chemical reaction fields and thus influence the dynamics of the whole system. In this paper, we consider a model of chemotactic particle coupling with nonlinear chemical reaction fields. Intriguingly, we find the aggregation of particles occurs when they consume substances and move toward high-concentration areas, which is quite counterintuitive. In addition, dynamic patterns can also be found in our system. These results imply that the interaction between chemotactic particles and nonlinear reactions can result in much novel behavior and may further extend to explain the complex phenomena in certain systems.

1 Introduction

Chemotaxis refers to the directional movement of particles in response to a specific chemical stimulus. Chemotactic particles are a class of particles that are widely present in practical systems. Due to their response to chemical stimuli, they can perform organized activities in complex environmental systems. In a variety of biological systems, chemotactic particles play an irreplaceable and important role.[1] For example, chemotaxis can lead to patterns or traveling bands formed by bacteria,[2–4] initial clusters of mesenchymal cells in embryonic development,[5,6] and chemotactic cytokines in the immune system which can promote immune responses.[7–9]

At present, the research on chemotactic particles can be divided into the following categories. The first one is derived from the behavior of bacteria in nature.[10–15] Keller and Segel's early research[16] suggested that the positive feedback loop between the signal release and chemotaxis of particles was the key to the formation of clusters. It has become a very popular direction to discuss the patterns formed by chemotactic particles under different chemical stimuli through the Keller-Segel approach. For example, Baronas *et al.* used a model to study the complex spatiotemporal patterns formed by *E. coli* in the presence of both nutrients and chemokines, which are very similar to the bioluminescence patterns observed in the experiment.[10] Another topic is to investigate the chemotactic Janus particles from artificial synthesis.[17–21] For example, B. Liebchen found that chemoattractive particles will form a single large cluster, while chemorepulsive particles will form size-limited clusters due to Janus instability or traveling wave with delay-induced instability.[17] Moreover, due to the prevalence of multi-component systems in the real world, recent studies have also focused on theoretical models composed of several components.[22–26] For example, J. Grauer *et al.* found that there is a swarm hunting phenomenon in the system consisting of two types of chemotactic particles. They also captured cluster ejections and other interesting phenomena.[22]

In the above systems, chemicals are generated by chemotactic particles and evolve mainly through a simple decay process. However, there are more complex effects in the actual system. The chemotactic particles themselves may produce or consume certain substances through catalytic reactions or biochemical processes. Chemical substances can also interact with each other through complex nonlinear reaction processes. Such cases can be found in certain biological systems. For example, during cancer invasion of tissues, there is a nonlinear proteolysis reaction between uPA and ECM, resulting in a heterogeneous distribution of cancer cells.[27] For another example, in the process of feather morphogenesis, there are nonlinear interactions of substances such as epithelial, FGF, and BMP, which mediate the formation of special feather morphogenesis.[28] Also, nonlinear dynamics have been used in designing self-organized motion,[29,30] coupled self-motion and chemical reaction are studied both theoretically and experimentally. It can be seen that the interplay between particles and chemical fields, combined with the nonlinear

Department of Chemical Physics & Hefei National Research Center for Physical Sciences at the Microscale & Key Laboratory of Precision and Intelligent Chemistry, University of Science and Technology of China, Hefei, Anhui 230026, China.
E-mail: hjjiang3@ustc.edu.cn, hzhlj@ustc.edu.cn

† Electronic supplementary information (ESI) available. See DOI: https://doi.org/10.1039/d2sm01433e

nature of the chemical reaction, can produce a wealth of phenomena. However, how the property of particles can influence the behavior of such a system has not been systematically studied.

Motivated by this, this paper presents a theoretical framework combining particle's chemotaxis and consumption/release of substances with nonlinear chemical reactions. We study the different phenomena that occur in systems when particles produce/consume and move towards/away from chemical species with different intensities. Surprisingly, we found that when chemotactic particles consume and move toward a substance, they can also form static clusters. This phenomenon is very counterintuitive and cannot be explained by the mechanism in the above-mentioned studies. This shows that the nonlinear process of the system plays a very important role in the clustering mechanism in this system. Also, the rate of production/consumption can dramatically affect the behavior of the system, which also shows the singularity of the system.

This paper consists of the following parts. In Section II we describe the simulation model of the system. The third section presents the main results and discussion. Finally, we summarize in section IV.

2 Simulation model

We consider a two-dimensional system consisting of one type of isotropic chemotactic particle and two chemical components U and V, as shown in Fig. 1.

To describe the motion of colloidal particles with radius σ, we adopt the Langevin equation as shown in eqn (1). Colloidal particles can be chemotactic to both substances, as shown in the upper part of Fig. 1. Details of chemotactic motion need specific description of the interaction between particle and liquid environment.[29] To be simple and more general, in this work, we consider a simple representation of chemotaxis, the case where the speed of the chemotactic movement of the particles is proportional to a linear order of concentration gradient of the substance ($\alpha_u\nabla c_u$ and $\alpha_v\nabla c_v$), where the coefficients (α_u,α_v) represent chemotactic strength. This form of chemotaxis has been widely used in studying synthetic chemotactic particles[22,31] and chemotaxis in biological system.[32,33] At this setting, the velocity of the chemotactic motion of the particles follows the direction of the concentration gradient. Taking U as an example, if $\alpha_u > 0$, the particle will move towards the high concentration region of U. Conversely, if $\alpha_u < 0$, the particles will move towards the low concentration region. WCA potentials, $V_{\mathrm{WCA}}(r_{ij}) = 4\varepsilon\left[\left(\frac{\sigma}{r_{ij}}\right)^{12} - \left(\frac{\sigma}{r_{ij}}\right)^{6} + \frac{1}{4}\right]$ if $r_{ij} < 2^{1/6}\sigma$ and zero otherwise, are used between the particles to represent volume exclusion effects,[34] in which r_{ij} represents the distance between a pair of particles and ε controls the strength of potential. $V = \frac{1}{2}\sum_{i,j\neq i} V_{\mathrm{WCA}}(|r_i - r_j|)$ is the sum over all particle pairs. $\boldsymbol{\eta}_i$ represents unit-variance Gaussian white noise with zero mean, which accounts for thermal motion of colloid.

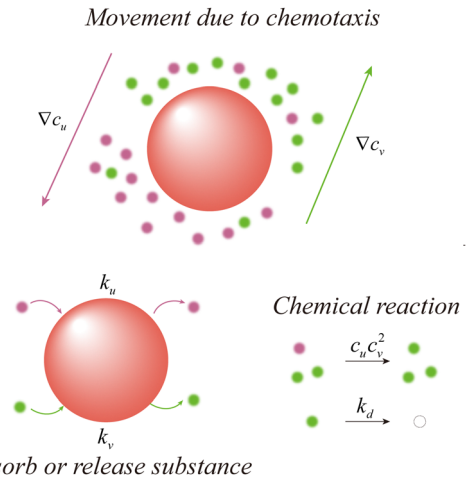

Fig. 1 Model of our system. The pink sphere refers to the chemotactic particle. Substances U and V are represented in purple and green, respectively.

For the modeling of chemical reactions, as mentioned earlier, we wanted to study nonlinear chemical reactions maintained far from equilibrium. We chose a simple autocatalytic reaction in an open system, involving a three-molecule autocatalytic reaction ($U + 2V \rightarrow 3V$), an external supply of reactant U and decay of the products V ($V \rightarrow P$). This model has been studied in depth and is known as Gray–Scott model.[35] We use Gray–Scott model here as a representative model of the behavior of high order nonlinear reaction in open system. With its bistable property, various patterns have been found based on the different stability of steady-state solutions. In this work, we mainly exploit its nonlinear characteristics and therefore choose its stable uniform state as the initial state of reaction fields.

The reaction rate is given by the law of mass action, which is $k_{\mathrm{reaction}} = c_u c_v^2$. The feeding flow of substance U at a rate k_f aims to maintain the level of U towards unit concentration 1. Product V has a constant decay rate k_d. Colloid particles may also produce or consume substances U and V at different rates, k_u and k_v, where positive rates represent production and negative ones represent consumption. The evolution equations are summarized as follows:

$$\frac{\partial \mathbf{r}_i(t)}{\partial t} = \alpha_u\nabla c_u + \alpha_v\nabla c_v - \nabla_{r_i} V + \sqrt{2D_p}\boldsymbol{\eta}_i \quad (1)$$

$$\frac{c_u(t)}{\partial t} = D_u\nabla^2 c_u - c_u c_v^2 + k_f(1 - c_u) + k_u\sum_i \delta(\mathbf{r} - \mathbf{r}_i) \quad (2)$$

$$\frac{c_v(t)}{\partial t} = D_v\nabla^2 c_v + c_u c_v^2 - k_d c_v + k_v\sum_i \delta(\mathbf{r} - \mathbf{r}_i) \quad (3)$$

In terms of parameters, we set $D_p = 0.1$, $D_u = 0.5$, $D_v = 0.25$, and the rate constant was taken as $k_f = 0.03$, $k_d = 0.08$. With this parameter, the original Gray–Scott model is in a stable uniform

state, calculated to be $c_u^0 = 0.32$, $c_v^0 = 0.25$. The interaction strength of WCA potential ε is set to 1. We numerically solve the equations in a two spatial dimensional (2D) box with $L = 300$ with periodic boundary conditions. The number of particles N is set to 7200. We use central differences for Laplace terms and forward Euler method for time integration. In the initial state, the particles are randomly distributed in space and the concentrations of the two substances are small random perturbations on the basis of the uniform state ($c_u^0 = 0.32$, $c_v^0 = 0.25$).

3 Results and discussion

3.1 Abnormal cluster formation

For simplicity, we only consider the case when particles interact with substance U in this work, which means $\alpha_v = 0$, $k_v = 0$ in the following. We first studied the case when the particles consume substance U and tend to U *i.e.* $\alpha_u > 0$, $k_u < 0$, which can correspond to particles chasing nutrients or immune cells killing antigens, *etc.*

Firstly, we fix the chemotactic strength $\alpha_u = 5.0$ and change the rate of consumption k_u. When $k_u = 0$, the chemical substances remain uniform and chemotaxis does not take effect, resulting in randomly distributed particles, as shown in Fig. 2a. As we gradually decrease k_u, when k_u is small enough, we find island-like clusters consist of colloidal particles, while the concentration distribution of substance U is also non-uniform (see Movie S1, ESI† and Fig. 2b–d). As shown in Fig. 2b–d ($k_u = -0.01$(b), -0.015(c), -0.02(d)), the size and number of the cluster structure in the final state vary with k_u. As k_u is smaller, the number of clusters formed in the final state is smaller and the size of clusters is larger. This is corroborated by the statistical plot in Fig. 2f, where the system appears with a larger number of small clusters when k_u is larger. When k_u is small, the clusters are connected into a whole, and in the extreme case, the particles of the whole system form a connected pattern ($N = 1$). In the snapshot Fig. 2b–d, we also observe a non-uniform distribution of the concentration field. So, we calculated the spatial distribution of the chemical substance U. As shown in Fig. 2e, the concentration distribution of the system becomes more inhomogeneous gradually (from the blue line to the red line) as k_u gradually becomes smaller. At $k_u = -0.03$, U shows a bimodal distribution of high and low concentrations. This indicates that particles aggregate to form cluster structures, but also the substances show a phase separation of high and low concentration.

A very counter-intuitive aspect of these results is that the constant consumption of substance U by the particles generally results in a concentration sink of substance U, which then drives the particles away from the sink area due to chemotaxis, which will not induce cluster formation. However, in our model, the particles form a static cluster with positive chemotaxis and constant consumption rate ($\alpha_u > 0$, $k_u < 0$). This phenomenon deserves further analysis. We take the white spline area in Fig. 2c to look at the detailed structure of clusters. We plot the spatial distribution of the concentration of matter U and V as well as the particle density in Fig. 3a. It can be seen that in the cluster region, the distribution of substance U shows a peak shape, while the distribution of V is just the opposite. Therefore, due to the chemotaxis of the particles, the particles gather at the peak position of the concentration field. However, considering the diffusion of U and V (arrows in Fig. 3a) and the consumption of U by the particles, this structure seems to be unsustainable. It is important to note that the feed of U will not lead to the formation of high-concentration areas. It can be seen from eqn (2), as k_u decreases, the steady state concentration will also decrease.

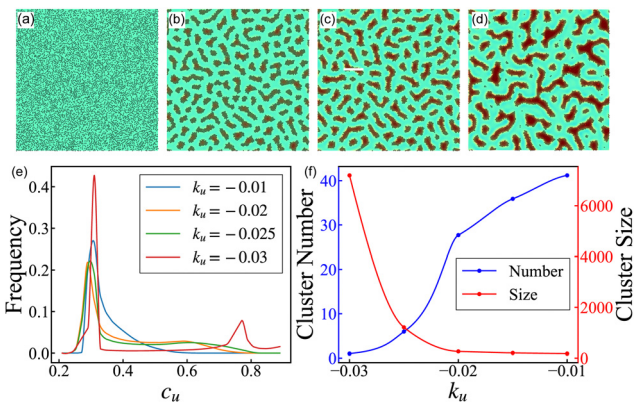

Fig. 2 Clusters formation when particles consume substance U. (a)–(d) Snapshot of the system at $t = 1000$, black spheres refer to particles and background color refers to the concentration of U (red for high concentration and green for low one). (a)–(d) Corresponds to $k_u = 0.0$, -0.01, -0.015, -0.02 respectively. (e) The variation of cluster number (blue line) and cluster size (red line) of particles with respect to k_u. (f) The concentration distribution of substance U under different k_u.

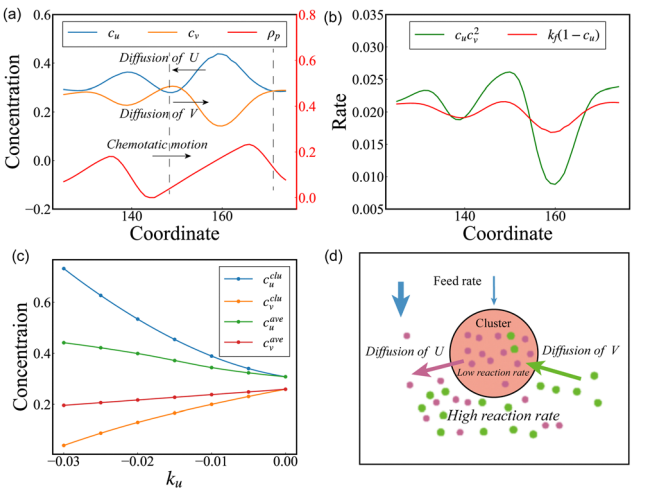

Fig. 3 Property of clusters. (a) The concentration profile of the system on the white line strip in Fig. 2c. Blue, orange, and red lines refer to the concentration of U and V (left axes), and the density of particles (right axes), respectively. (b) The calculated reaction rate (green line) and feed rate (red line) on the area same as (a). (c) Average concentration on the whole system (green for U and red for V) and near particles (blue for U and orange for V) of U and V. (d) Cluster illustrations. Substances U and V are represented in purple and green, respectively. The feed rate of U is represented in blue arrows.

We must therefore consider the effect of chemical reactions between U and V to explain the formation of the cluster pattern.

We calculated the feed rate and reaction rate in the same region, as shown in Fig. 3b. Interestingly, inside the cluster, the rate of the chemical reaction is lower than the feed rate, while outside the cluster, the rate of the chemical reaction is higher than the feed rate. This explains why the clusters can be stable because the gap between the feed and the reaction compensates for the diffusion effect. This difference in concentration between inside and outside clusters is present for all clusters in the system. To visualize this effect, we calculate the average concentration of two substances globally and in the region of cluster formation, the results are shown in Fig. 3c. It can be seen that the concentration of substance U inside the cluster (c_u^{clu}) is always higher than the average concentration of the whole system (c_u^{ave}), while the concentration of V (c_v^{clu}) is always lower than the average concentration of the system (c_v^{ave}). Therefore, we can attribute the structure of the static cluster to Fig. 3d. Inside the cluster, the feed rate is small, but the reaction rate is smaller or even close to zero, and a large amount of substance U is accumulated and can then be consumed by the particles. Meanwhile, outside the cluster, although the feed rate is larger, a large amount of material U is converted to V by the reaction, so the concentration of U is still low and the particles will not leave the cluster region.

Above we understand the reason why the clusters can exist stably, but another important question is how the system evolves into this final form, *i.e.*, how the system with a random initial state evolves into a non-uniform cluster structure. This can be found in the dynamic process of system evolution. A natural idea is that particle consumption causes concentration fluctuations in the concentration field, so we followed the concentration evolution near a single particle, as shown in Fig. 4a, and also calculated the corresponding feed and reaction rates, as shown in Fig. 4c. The kinetic process can be divided into three regimes according to their characteristics. In regime I, when the particle consumes the substance U causes a transient decrease in its concentration. This causes a decrease in the reaction rate, so the concentration of V starts to decrease, while the concentration of substance U does not decrease much due to the continuous feed (red line in Fig. 4c). When entering Regime II, the decrease in V brings about a rapid decrease in the reaction rate ($k = c_u c_v^2$ shown in Fig. 4c green line). This causes an accumulation of substance U, while V decreases rapidly or even tends to 0 due to the decrease in the reaction rate, which is the only source of V. At this point, chemotaxis causes particles to accumulate in the area of high U concentration, further exacerbating the change. Subsequently, due to the reaction and the movement of the particles cannot stop suddenly, substance U begins to excessive accumulation, along with the diffusion effect, the concentration of U begins to decline after reaching the peak, and the concentration of V gradually increases (see the beginning of Regime III). This increases the rate of chemical reaction, further decreasing U and increasing V. This cycle leads to a convergence towards the final steady state *i.e.*, the final stationary state (late stage of

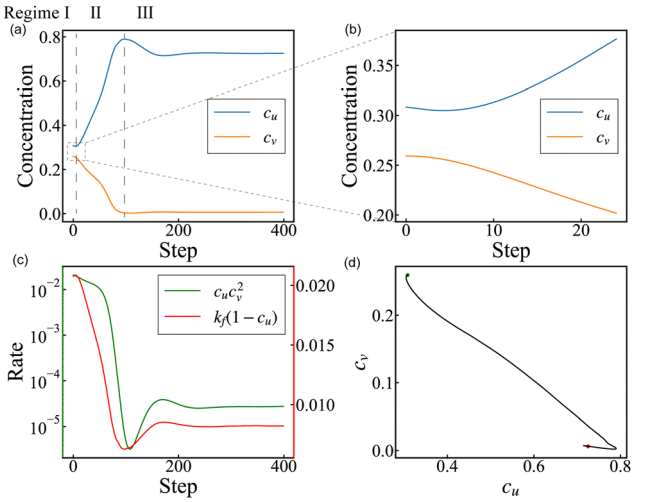

Fig. 4 Dynamics of clusters formation. (a) The concentration of U and V near a certain particle of the system with respect to simulation time. (b) Enlarged image for t = 0–25 of (a). (c) The reaction rate (green line) and feed rate (red line) evolution curve. (d) The trajectory of concentration evolution.

Regime III). The trajectory from the green point to the red point shown in Fig. 4c also demonstrates this process.

It can be seen that such a cluster formation mechanism is significantly different from the ones in the previous studies, such as K–S instability or Janus instability.[17] The first one requires that particles produce matter and tend to it $\alpha_u > 0$, $k_u > 0$, while the latter is due to asymmetric particles producing matter and repelling it, which means $\alpha_u < 0$, $k_u > 0$. We can briefly describe our mechanism as following steps:

- Consumption of the substance U by the particles.
- Decrease in the reaction rate.
- Accumulation of U and decrease in V.
- Chemotactic motion of particles.

The key point of this mechanism is the nonlinear property of reaction. The consumption of substance U will trigger the nonlinear nature of the reaction, fluctuations in concentration will not recover directly but will continue to evolve to a new steady state. The systematic stability analyses will be carried out later.

3.2 Dynamic Inhomogeneous Pattern

From the previous section we see that the consumption of particles leads to an increase in the concentration of U, then the aggregation of particles is observed. Using this mechanism, if we consider the case when $\alpha_u < 0$, $k_u < 0$, which means particles consume U and avoid it. Analogous to the previous phenomenon, it can be inferred that the particles will be constantly caught in the cycle of "consumption of substance U" – "increase in concentration of U" – "chemotactic movement towards low concentration". Therefore they may perform a directional motion and will not form a stable cluster. To test this idea, we simulate the situation when the particle $\alpha_u < 0$, $k_u < 0$. We find that when k_u is close to zero, the system remains in a uniform state. However, when k_u is small enough,

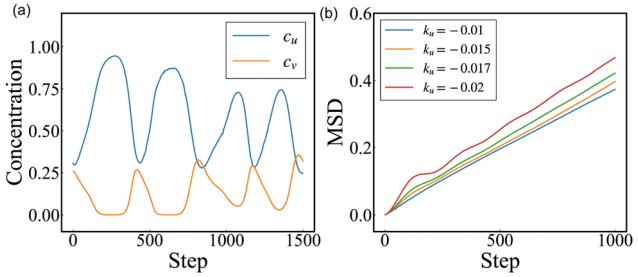

Fig. 5 Changes in concentration over time when $\alpha_u < 0$, $k_u < 0$. (a) Typical time series of U and V at the observation point. (b) Mean square displacement of particles in the system with different k_u. MSD lines of particles are averaged with 40 different initial configurations.

the concentration of substance U and V get out of uniform state and starts to change over time. It is worth mention that the system is not homogeneous, thus the particles are moving correspond to substance due to chemotaxis.

We plot the time series of the concentrations at a given point in the system (Fig. 5a), we can see that the concentrations of the two substances U and V change over time, with the peaks and troughs of the two substances being opposite to each other. The concentration of U is high where the concentration of V is low. The MSD image of the particle motion was calculated (Fig. 5b). We can see, for large k_u, the MSD curve shows significant oscillation in the early stage, which also indicates the directional motion of the particles in a short time stage. These results suggest that the mechanism described in the previous section, *i.e.*, the nonlinear effect of reaction triggered by particle, still holds. With $k_u < 0$, and the particle causes the concentration of substance U to increase, and then due to chemotaxis ($\alpha_u < 0$), it moves to a region with a low concentration of U. It then causes an increase in the concentration of substance U in that place. This mechanism is similar to the "Delay induced instability",[17] in which chemotactic Janus particles may oscillate due to excessive accumulation of chemical substance. The difference is that, in this work, particles consume the substance and result in a concentration increase through a chain of nonlinear chemical reactions, while in "Delay induced instability"[17] particles need to release the substance to create areas of high concentration.

3.3 Phase diagram and linear stability analysis

In order to get a global picture of the system under different parameters, we plot the phase diagram in the α_u–k_u plane, as shown in Fig. 6. We divide the states of system into three types, uniform, static pattern, and dynamic pattern according to concentration distribution of U and V. The first one is homogeneous, while the last two are inhomogeneous. To identify whether the system is uniform, we record the spatial distribution of substance U and calculated the variance in the late stage of the simulation. States with small enough variance (<0.001) are uniform states. For the inhomogeneous states, in order to distinguish between static and dynamic states, the time series of U are used. The steady state of concentration similar to

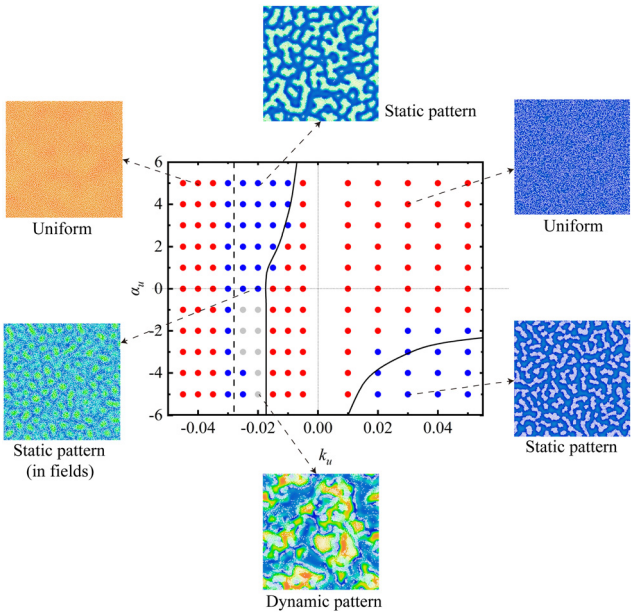

Fig. 6 Phase diagram of system in α_u–k_u space. Points are used to differentiate between different states of the system. Red points refer to the uniform state, blue points refer to static inhomogeneous pattern and gray points refer to the dynamic inhomogeneous pattern. Lines are transition lines of different states in the continuous system. The solid line is the boundary of instability in the continuous system. The dashed line indicates the bounds on whether the system has non-trivial homogeneous solutions. Background color in snapshots represents concentration of U with orange for high concentration and blue for low concentration.

Fig. 4(a) marks a static pattern while a variation of concentration with time like in Fig. 5(a) marks an inhomogeneous dynamic pattern.

Different colors of points in Fig. 6 represent different states of the system in the late stage of simulation. The red color indicates that the system is in a uniform state, with uniform fields and randomly moving particles. For the inhomogeneous states, the blue color represents the formation of static clusters in fields, and the grey color indicates that the system is in a dynamic inhomogeneous pattern, accompanied by continuous changes in concentration over time and directional motion of particles. The snapshots around the phase diagram correspond to the parameters represented by the points, and we have indicated this correspondence with arrows. In the following, we analyze the different areas of the phase diagram in detail in order to obtain a more comprehensive characterization of this system.

Firstly, when $\alpha_u = 0$, the particles are pure consumers of substance U without chemotactic motion. With a smaller enough $k_u < 0$, the uniform fields lose stability and spatial pattern forms, while particles are still uniformly distributed as shown in snapshots in Fig. 6. Note that, in this case, the origin of this pattern is consistent with the instability behavior of the chemical reaction field without particles. According to the stability analysis of the original Gray–Scott model,[36] our parameter of k_f and k_d is near the Hopf bifurcation line. As the uniformly distributed particles (when $\alpha_u = 0$, $k_u < 0$) effectively

decrease the k_f, the system goes beyond the bifurcation line and loses stability.

Beyond the x-axis of the phase diagram, when $\alpha_u \neq 0$, chemotaxis comes into play. As shown in Fig. 6, with $\alpha_u > 0$, the threshold of cluster formation is much bigger than the threshold at $\alpha_u = 0$. In the region of $\alpha_u > 0$, $k_u < 0$, if the cluster structure can form, the particles need to consume enough U so that the reaction rate decreases to trigger instability, else if the consumption rate is too small, other factors such as diffusion are sufficient to bring the system back to the steady state. Thus, the system is stable when k_u is small and destabilized when it is large. The other influencing factor is α_u, because particles with chemotaxis can aggregate to further drive the system away from the steady state. With larger α_u, a lower consumption rate is needed to form clusters. In the region of $\alpha_u < 0$, $k_u < 0$, similarly, a large enough consumption rate is required to induce a dynamic inhomogeneous pattern.

However, for too large consumption rates $k_u < -0.03$, the concentration of V decreases rapidly to 0 and the concentration of U then increases to near 1. Without concentration gradient, the particles would not gather and maintain random uniform distribution.

For the $k_u > 0$ region, the particles release U, resulting in a low-concentration region of U. If the particles tend to the low-concentration region, *i.e.* $\alpha_u < 0$, cluster structures will form, this is similar to the situation of $\alpha_u > 0$, $k_u < 0$.

To further understand the overall behavior of our model, the system was rewritten in continuum description and subjected to linear stability analysis (LSA).[22] The equations of the continuous system are as follows:

$$\frac{\partial \rho(t)}{\partial t} = D\Delta\rho - \alpha_u \nabla \cdot (\rho \nabla c_u) - \alpha_v \nabla \cdot (\rho \nabla c_v) \tag{4}$$

$$\frac{c_u(t)}{\partial t} = D_u \Delta c_u - c_u c_v^2 + k_f(1 - c_u) + k_u \rho \tag{5}$$

$$\frac{c_v(t)}{\partial t} = D_v \Delta c_v + c_u c_v^2 - k_d c_v + k_v \rho \tag{6}$$

The ρ refers to the density of chemotactic particles, and c_u, c_v means concentration of substances U and V, respectively. We perform a linear stability analysis around the stationary solution (ρ_0, u_0, v_0), which represents the uniform state of the system. We apply a small plane wave perturbation with wavenumber q around the stationary solution and solve for the dispersion relation of these fluctuations in Fourier Space, denoted as $\lambda(q)$. If $\mathrm{Re}[\lambda(q)] < 0$ holds for all q, the continuous equation is stable and the perturbation applied to uniform solution is gradually recovered. Conversely, as long as there exists any q' such that $\mathrm{Re}[\lambda(q')] > 0$, the steady-state solution is destabilized and the system is unstable under certain perturbation, patterns may emerge in this case.

On the left side of the vertical dashed line in Fig. 6, only a trivial solution ($\rho = \rho_0$, $u = 1$, $v = 0$) exists and no patterns can be found. On the right side, we calculate $\lambda(q)$ with varying k_u and α_u and find the bounds of the stable and unstable regions, as shown in the solid black line in Fig. 6. Detailed dispersion relation graphs are shown in Fig. S1 in ESI.† Note that when $\alpha_u = 0$ Hopf bifurcation occurs when k_u decreases, like in original Gray–Scott system.[36] For $\alpha_u > 0$, we find a finite domain in q for which $\mathrm{Re}((q)) > 0$ when uniform solution is unstable, which indicates Turing instability. As for $\alpha_u < 0$, Hopf bifurcation is found when $k_u < 0$, but when $k_u > 0$ there is also Turing instability.

These results suggest that the introduction of chemotaxis can dramatically change the nature of a nonlinear reaction system. Chemotaxis regulates the system so that different static or dynamic patterns are presented. Moreover, these results are consistent with particle simulations. In the region of Turing instability, $\alpha_u > 0$, $k_u < 0$ and $\alpha_u < 0$, $k_u > 0$, Turing pattern is also found in particle simulation. For the region beyond Hopf bifurcation when $\alpha_u \leq 0$, $k_u < 0$, uniform states are unstable and we can predict that patterns may emerge. As shown in simulation, when $\alpha_u = 0$, $k_u < 0$, inhomogeneous static patterns only in fields are found. When $\alpha_u < 0$, $k_u < 0$, despite only Hopf bifurcation is found in LSA in this region, inhomogeneous dynamic patterns emerge in simulations. We can see that for all regions where the uniform solution is unstable in LSA, we can find patterns that emerge in the simulation.

Furthermore, we find that the transition line given by the linear stability analysis (solid black line) is very close to the boundary obtained from the particle simulation. Since the effect of particle volume is not considered in the continuous equation, there is a difference in the location of boundaries, but the agreement in the qualitative shapes of the boundaries illustrates the correctness of our proposed mechanism.

4 Conclusions

In summary, we combine the chemotactic effects of particles with nonlinear reactions and find that there are dynamic and static patterns in the system due to a combined effect of particle and substance coupling with nonlinearity. One of the most interesting parts is that, while particles consuming substances cause a concentration decrease in the whole system, they can form a substance-enriched cluster. This can be an important mechanism for biological systems to achieve specific functions, such as the enrichment and elimination of antigens or aggregation of nutrients. From another point of view, we obtain a phase-separated reaction system with high and low-density phases and maintained in a stationary state. The reaction rate is different inside and outside the clusters. Similar phenomena can be seen in systems where active chemical reactions and phase separation are combined.[37,38] Notably, we demonstrate a mechanism that the consumption of certain substance triggers the nonlinearity effect of reaction, which drives the system towards a heterogeneous state. We also consider other parameter regions and find the dynamic pattern of the system which can also be understood in a similar mechanism.

Currently, we only consider the effects caused by the interaction with the substance U. Since U and V are mutually coupled, particles that interact with V can also form a series of special phenomena. Obviously, Gray–Scott model can not represent all of nonlinear reaction models. It is a bistable medium and is located near the bifurcation line at the parameters chosen in this work. If we consider other nonlinear systems, such as the ones that exhibit spiral waves or chemical chaos, chemotactic particles can also interact with them to form various structures. Although, same ''abnormal pattern'' may not emerge in all of these nonlinear reactions, the interplay of chemotaxis and nonlinear reaction will induce many intriguing phenomena. For example, in excitable media, such as FitzHugh–Nagumo model, excitation triggered by chemotaxis may be an interesting behavior. Also, for the present system, we only consider simple, symmetric chemotactic particles, but if we further consider active particles such as chemotactic Janus particles,[39] the coupling of activity, nonlinearity, and anisotropic effect will lead to more complex states of such systems. There are now also many experiments using nonlinear reactions to achieve self-propel,[30] and such systems also have many interesting properties that deserve further study. These problems can be investigated in the future.

Conflicts of interest

There are no conflicts to declare.

Acknowledgements

This work is supported by MOST (2022YFA1303100), NSFC (21833007, 32090040).

References

1 G. H. Wadhams and J. P. Armitage, *Nat. Rev. Mol. Cell Biol.*, 2004, **5**, 1024–1037.
2 D. F. Blair and H. C. Berg, *Science*, 1988, **242**, 1678–1681.
3 A. d'Onofrio, *J. Theor. Biol.*, 2012, **296**, 41–48.
4 P. J. Van Haastert and P. N. Devreotes, *Nat. Rev. Mol. Cell Biol.*, 2004, **5**, 626–634.
5 M. Mimura and T. Tsujikawa, *Physica A*, 1996, **230**, 499–543.
6 S. W. Moore, M. Tessier-Lavigne and T. E. Kennedy, *Netrins and Their receptors*, Springer, New York, New York, NY, 2007, pp. 17–31.
7 J. W. Griffith, C. L. Sokol and A. D. Luster, *et al.*, *Annu. Rev. Immunol.*, 2014, **32**, 659–702.
8 R. Gillitzer and M. Goebeler, *J. Leukocyte Biol.*, 2001, **69**, 513–521.
9 P. Hunter, *EMBO Rep.*, 2012, **13**, 968–970.
10 R. Baronas, Ž. Ledas and R. Šimkus, *Nonlinear Anal.: Modell. Control*, 2015, **20**, 603–620.
11 H. G. Othmer, X. Xin and C. Xue, *Int. J. Mol. Sci.*, 2013, **14**, 9205–9248.
12 N. Bellomo, A. Bellouquid, Y. Tao and M. Winkler, *Math. Models Methods Appl. Sci.*, 2015, **25**, 1663–1763.
13 G. Estrada-Rodriguez, H. Gimperlein and K. J. Painter, *SIAM J. Appl. Math.*, 2018, **78**, 1155–1173.
14 B. Perthame, N. Vauchelet and Z. Wang, *Rev. Mat. Iberoam.*, 2019, **36**, 357–386.
15 E. Rocca, G. Schimperna and A. Signori, arXiv, preprint, arXiv:2202.11007, 2022.
16 E. F. Keller and L. A. Segel, *J. Theor. Biol.*, 1971, **30**, 225–234.
17 B. Liebchen, D. Marenduzzo, I. Pagonabarraga and M. E. Cates, *Phys. Rev. Lett.*, 2015, **115**, 258301.
18 B. Liebchen, M. E. Cates and D. Marenduzzo, *Soft Matter*, 2016, **12**, 7259–7264.
19 R. Singh, R. Adhikari and M. Cates, *J. Chem. Phys.*, 2019, **151**, 044901.
20 O. Pohl and H. Stark, *Phys. Rev. Lett.*, 2014, **112**, 238303.
21 I. Theurkauff, C. Cottin-Bizonne, J. Palacci, C. Ybert and L. Bocquet, *Phys. Rev. Lett.*, 2012, **108**, 268303.
22 J. Grauer, H. Löwen, A. Beer and B. Liebchen, *Sci. Rep.*, 2020, **10**, 1–11.
23 R. Soto and R. Golestanian, *Phys. Rev. Lett.*, 2014, **112**, 068301.
24 J. Agudo-Canalejo and R. Golestanian, *Phys. Rev. Lett.*, 2019, **123**, 018101.
25 B. Nasouri and R. Golestanian, *Phys. Rev. Lett.*, 2020, **124**, 168003.
26 K. Shrinivas and M. P. Brenner, *Proc. Natl. Acad. Sci. U. S. A.*, 2021, **118**, e2108551118.
27 M. A. Chaplain and G. Lolas, *Networks Heterog. Media*, 2006, **1**, 399.
28 K. J. Painter, W. Ho and D. J. Headon, *J. Theor. Biol.*, 2018, **437**, 225–238.
29 S. Nakata, V. Pimienta, I. Lagzi, H. Kitahata and N. J. Suematsu, *Self-organized Motion: Physicochemical Design based on Nonlinear Dynamics*, The Royal Society of Chemistry, 2018.
30 N. J. Suematsu, Y. Mori, T. Amemiya and S. Nakata, *J. Phys. Chem. Lett.*, 2016, **7**, 3424–3428.
31 J. L. Anderson, *Annu. Rev. Fluid Mech.*, 1989, **21**, 61–99.
32 J. D. Murray, *Mathematical biology II: Spatial models and biomedical applications*, Springer, New York, 2001, vol. 3.
33 H. Knútsdóttir, E. Pálsson and L. Edelstein-Keshet, *J. Thero. Biol.*, 2014, **357**, 184–199.
34 J. D. Weeks, D. Chandler and H. C. Andersen, *J. Chem. Phys.*, 1971, **54**, 5237–5247.
35 P. Gray and S. Scott, *Chem. Eng. Sci.*, 1983, **38**, 29–43.
36 J. S. McGough and K. Riley, *Nonlinear Anal.: Real World Appl.*, 2004, **5**, 105–121.
37 D. Zwicker, *Curr. Opin. Colloid Interface Sci.*, 2022, **61**, 101606.
38 J. Bauermann, S. Laha, P. M. McCall, F. Julicher and C. A. Weber, *J. Am. Chem. Soc.*, 2022, **144**, 19294–19304.
39 Z. Huang, P. Chen, G. Zhu, Y. Yang, Z. Xu and L.-T. Yan, *ACS Nano*, 2018, **12**, 6725–6733.

